Substorm growth and expansion onset as observed with ideal ground-spacecraft THEMIS coverage

V. Sergeev,[1] V. Angelopoulos,[2] M. Kubyshkina,[1] E. Donovan,[3] X.-Z. Zhou,[2] A. Runov,[2] H. Singer,[4] J. McFadden,[5] and R. Nakamura[6]

Received 18 May 2010; revised 25 October 2010; accepted 8 December 2010; published 4 February 2011.

[1] We present a fortuitous case of an isolated substorm on 29 March 2009, observed by the Time History of Events and Macroscale Interaction during Substorms (THEMIS) probes clustered at ~11–14 R_E with simultaneous coverage by the THEMIS ground network. The four probes are at roughly the same radial and azimuthal location, with one probe staying near the neutral sheet during entire growth phase and during the ensuing transition to the substorm expansion phase. Prior to substorm onset, THEMIS observed the damping of earthward convection and development of an embedded tail current sheet with half thickness ≤ 0.15 R_E and current density ~20 nA/m^2, while the total magnetic field closest to the neutral sheet was below 2 nT. Tail activity was observed to start prior to substorm onset tailward of the THEMIS probes (<-14 R_E) with the gradual increase of earthward flow and total pressure in front of an earthward moving bursty bulk flow event (BBF). There was no evidence of an outward propagating rarefaction wave prior to BBF onset. Peak flow was accompanied by two short dipolarization pulses, followed by a sharp reduction of the total pressure (up to 30–50%) and a decrease in the lobe magnetic field. By analyzing the lobe field waveforms, we infer their reconnection origin and argue that different onset-related magnetotail phenomena discussed in past literature (BBFs, bubbles, current disruption, nightside flux transfer events, earthward traveling convection regions) are views of the same dissipative structure formed by reconnection, when it is observed from different vantage points. Although the first ionospheric signatures of the substorm were observed near the equatorward edge of the auroral oval, the adaptive magnetospheric model maps the breakup to the tail current sheet at 15–20 R_E, consistent with other estimates of the substorm onset location available in our case. The event provides definite evidence in favor of tail reconnection within a thin current sheet as the primary substorm initiation process. It also demonstrates that actual changes of tail current magnitude in the magnetotail can be an order of magnitude larger, compared to the magnitude of 3-D current inferred from ground observations.

Citation: Sergeev, V., V. Angelopoulos, M. Kubyshkina, E. Donovan, X.-Z. Zhou, A. Runov, H. Singer, J. McFadden, and R. Nakamura (2011), Substorm growth and expansion onset as observed with ideal ground-spacecraft THEMIS coverage, *J. Geophys. Res.*, *116*, A00I26, doi:10.1029/2010JA015689.

1. Introduction

[2] During substorms the magnetotail configuration displays gross configurational changes that are of considerable importance for substorms and also of great interest in a plasmaphysical context. For isolated substorms, following the north-south IMF turning that initiates dayside reconnection and transport of the open magnetic flux into the tail, the tail current and its magnetic field grow during the growth phase providing energy storage for subsequent substorm expansion. During this stage the thin current sheet (TCS) appears to be embedded in the near-Earth plasma sheet and grows quickly, providing a potential place for different instabilities to occur. Finally, the configuration becomes unstable, and explosive instability occurs locally in

[1]Institute of Physics, St. Petersburg State University, St. Petersburg, Russia.
[2]Institute of Geophysics and Planetary Physics, University of California, Los Angeles, USA.
[3]Department of Physics and Astronomy, University of Calgary, Calgary, Alberta, Canada.
[4]NOAA Space Weather Prediction Center, Boulder, Colorado, USA.
[5]Space Science Laboratory, University of California, Berkeley, California, USA.
[6]Space Research Institute, Austrian Academy of Sciences, Graz, Austria.

0148-0227/11/2010JA015689

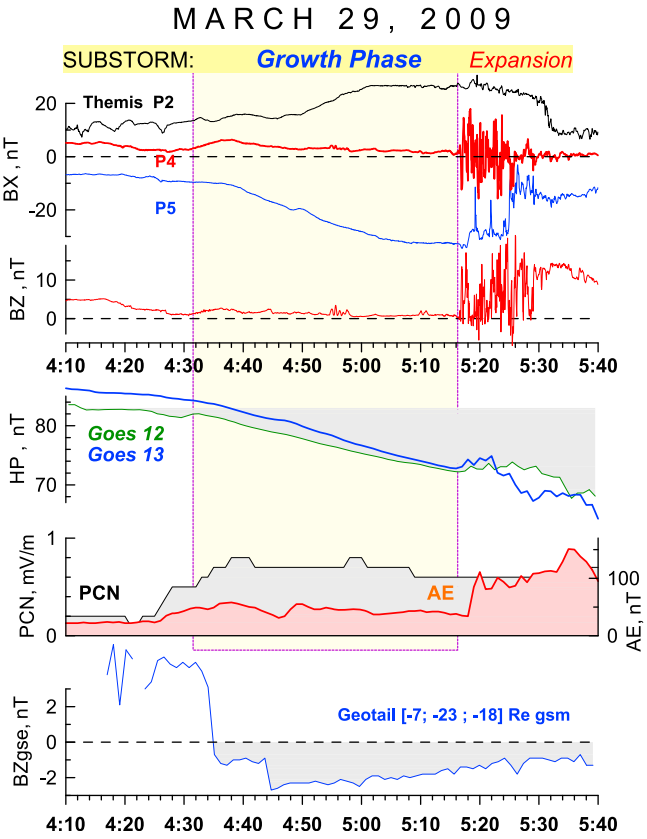

Figure 1. Survey of substorm event on 29 March 2009. From top to the bottom, B_x and B_z magnetic field components in the magnetotail (THEMIS P2, P4, P5 probes); H_p magnetic field component at near midnight (GOES 12 and 13 spacecraft); ground magnetic PCN (northern PC) and AE indices; and B_z component at Geotail spacecraft in the magnetosheath.

a still undetermined region of the plasma sheet, from which it propagates to other plasma sheet regions as well as to the ionosphere, indicating a substorm expansion phase. This observation-based picture, the basic elements of which were suggested a long time ago [*McPherron et al.*, 1973; *Nishida and Hones*, 1974] and later developed in many following studies, is incomplete; a number of important details and numbers are still missing.

[3] The main caveat of previous observational event studies, which addressed TCS formation and its disruption, is that the results are very sensitive to spacecraft location with respect to the TCS center plane (the neutral sheet), with very low probability for the spacecraft to stay in the neutral sheet. Since the TCS usually moves vertically [e.g., *Petrukovich et al.*, 2007], it is almost impossible to probe this region continuously. The same problem also strongly affects the quality of data-based magnetospheric modeling [*Kubyshkina et al.*, 2009] as well as the reliability of substorm onset determination and timing studies. As shown in some published examples, the initial region of substorm onset-related fast flow (bursty bulk flow, BBF) may occupy the very narrow central part of the thick plasma sheet, so even a spacecraft in the high-beta central plasma sheet (CPS) region within 1 R_E of the neutral sheet may miss the fast flow and accelerated plasma [see, e.g., *Sergeev et al.*, 2008, Figure 5].

[4] In this paper we present a unique observation in which the prebreakup growth of the embedded thin current sheet at 10–15 R_E as well as its subsequent disruption are monitored by a constellation of four closely spaced Time History of Events and Macroscale Interaction during Substorms (THEMIS) probes (P2–P5) in the region magnetically conjugate to the auroral breakup, with one remaining in the neutral sheet during the entire growth phase and the others bracketing the neutral sheet from two sides. In this study, the emphasis will be on TCS growth, onset location and timing, and the plasma structure of the disrupted current sheet at substorm onset. More details about the evolution of ion distribution functions and magnetospheric modeling/mapping in this event can be found in the companion papers by *Zhou et al.* [2010] and *Kubyshkina et al.* [2011], respectively.

[5] This event satisfies another requirement for a conclusive study. Its clear onset in ground-based magnetic and optical data indicates that THEMIS probes observed the plasma sheet near the central longitude of auroral breakup. Also, we take advantage of data-based adapted models capable of resolving the TCS and providing accurate mapping, a key point in ground-tail comparisons. Finally, excellent ground optical observations combined with DMSP observations provide a large-scale context for this study.

2. Observations

2.1. General Overview and THEMIS Growth Phase Observations

[6] The event on 29 March 2009 is an isolated substorm stimulated by southward turning of the IMF, which, according to Cluster observations (not shown), took place at about 0412 UT near subsolar bow shock; 20 min later it was also observed in the dawn magnetosheath by Geotail (see Figure 1). According to PCN and AE indices, at 0425 UT, the magnetosphere reacted by increasing convection; 5 min later, monotonic depression of the H component at geosynchronous orbit indicated the start of magnetic field stretching in the magnetotail. The growth of the tail current and its thinning were also monitored by THEMIS probes (see the increase in the B_x component absolute value at P2 and P5 in Figure 1). According to many types of observations (auroral, ground magnetic, THEMIS, and GOES, substorm expansion took place between 0516 and 0518 UT.

[7] This event occurred during a minor conjunction when four of five THEMIS spacecraft (P2–P5) were clustered in the local time sector 22.5–23 MLT in the near-Earth magnetotail between 11 R_E and 15 R_E. Geostationary spacecraft GOES 12 and GOES 13 extended the observation region down to 6.6 R_E. Spacecraft location plot in Figure 2 (top) demonstrate excellent coverage of the current sheet: P2–P5 are distributed in the Z coordinate within 1 R_E of both sides of the neutral sheet. According to observations (Figures 2 and 3), the B field magnitude at P4 stayed at low amplitude (<5 nT) throughout the entire growth phase and fell below ~2 nT at the end of it. This shows that P4 monitored the neutral sheet continuously during the entire growth phase, a very fortunate and extremely rare occurrence. The true location of the neutral sheet was therefore steadily ~0.5 R_E above the nominal

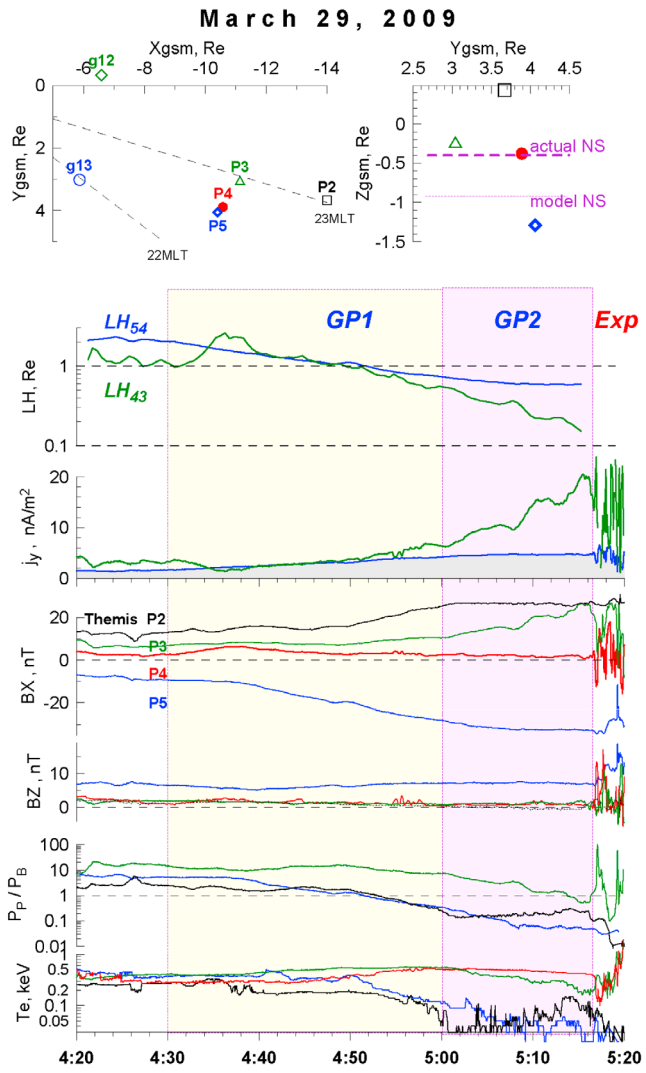

Figure 2. (top) GSM coordinates of magnetospheric spacecraft and (bottom) overview of THEMIS P2–P5 observations, including (from bottom to top) electron temperatures, ratio of plasma pressure to magnetic pressure, B_z and B_x GSM magnetic field components, estimates of cross-tail current j_y using differences of B_x components at pairs P3–P4 and P4–P5, and estimates of Harris current sheet thickness LH for the same pairs of spacecraft.

neutral sheet location (Figure 2, top), indicating an upward tilt of the tail current sheet. Such tilt is also evidenced by the positive B_z of 7 nT amplitude observed by P5 in the southern lobe/boundary layer plasma sheet (BLPS) region, which contrasts with the small B_z observed by three other probes, which remained above the neutral sheet (Figure 2).

[8] From 0430 until 0515 UT, P4 was at 11 R_E distance in the premidnight (22.5 MLT) magnetotail. Its observations (Figures 2 and 3) indicated very steady behavior of all parameters throughout the growth phase. The temperature was about 3 and 0.6 keV for protons and electrons, respectively. The total (actually plasma) pressure increased smoothly by 25% (from 0.31 to 0.39 nPa) during the first stage of the growth phase, mostly because of the density growth from 0.65 to 0.88 cm^{-3}. No considerable electric field or flows were observed. To characterize the average flux transport rate, we computed the average value of $[BV_i]_y$ (a proxy of E_y); between 0430 UT and 0515 UT it was about +0.01 mV/m. To our knowledge this is the first estimate of average earthward flux transport during the growth phase in the neutral sheet at the entry to the dipole-like magnetosphere.

[9] A fortunate feature of this event is that P5 was separated vertically from P4 by 0.92 R_E, whereas P3 was above P4 by only 0.16 R_E. This provided an opportunity to compare the experimental estimates of electric current density averaged over medium (~1 R_E) and small (~0.1 R_E) separations. The current density can be estimated in the slab between ith and jth probes as j_y^{ij} (nA/m^2) = 0.8 * $(B_X^i - B_X^j)$/$(Zns^i - Zns^j)$ if B is taken in nT and Z distance in thousand kilometers. At the beginning of the time interval two estimates agree and show current density ~2–3 nA/m^2 and Harris half thickness ~2 R_E (Figure 2), consistent with standard magnetospheric models. They grew nearly in parallel during the initial 20–30 min of the growth phase (GP1), but separated largely during its second part (GP2). Here the large-scale estimate saturates, but the small-scale current density grows explosively with superimposed ~5 min timescale variations. The saturation of the large-scale average current density (the saturation of the total current) seems to be a real effect supported by saturation of the total (plasma+magnetic) pressure at P2 and P5, which both stay in low-beta plasma (Figure 2). Toward the end of growth phase the explosively growing current density reached ~20 nA/m^2 and the Harris half thickness fell below to 0.15 R_E, only 6 times larger than the ion scale (both ion inertial length and thermal ion gyroradius in lobe field were about 250 km at that time).

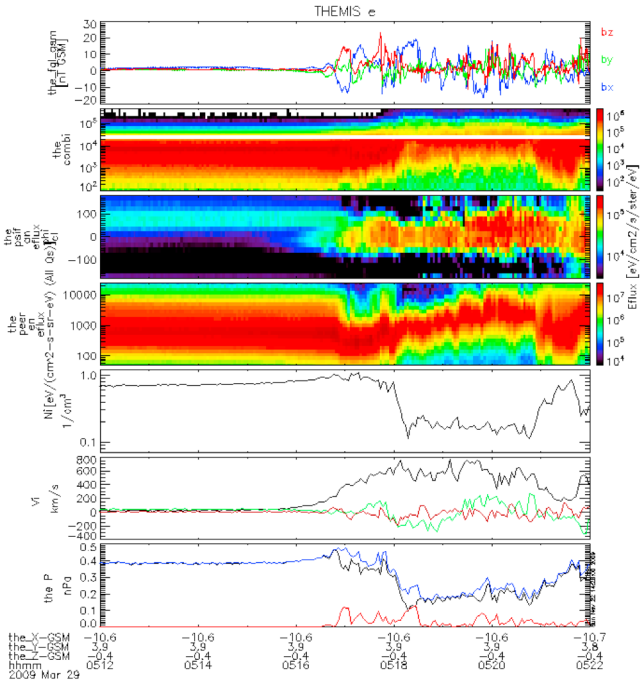

Figure 3. Survey of THEMIS P4 spacecraft observations.

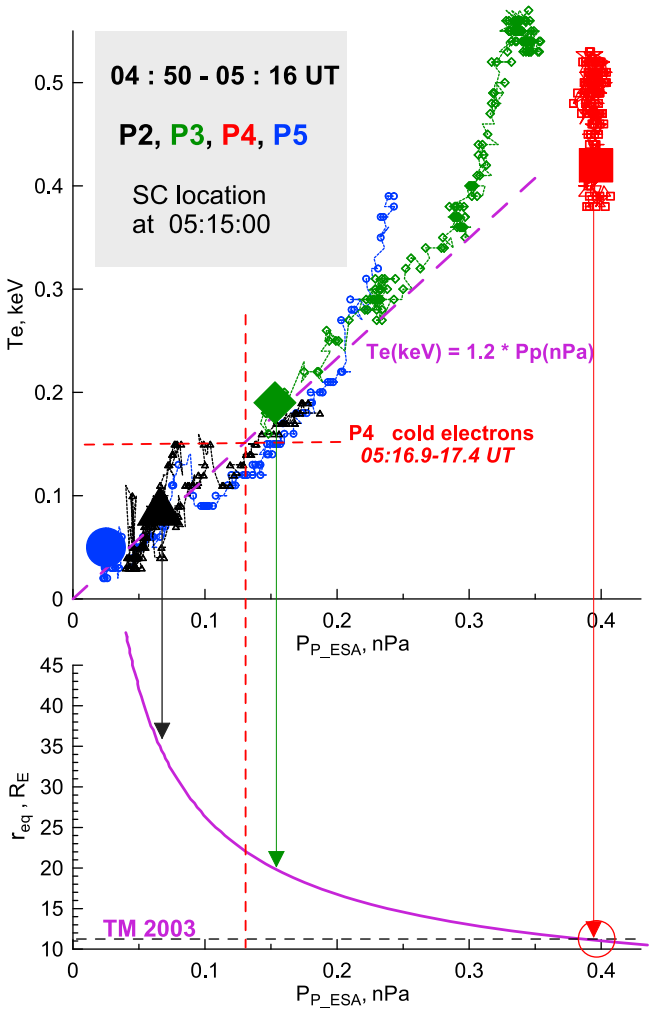

Figure 4. (top) Relationship between electron temperature and plasma pressure observed by THEMIS spacecraft during the substorm growth phase; large symbols indicate parameters at the end of the growth phase. (bottom) Radial dependence of plasma pressure according to [*Tsyganenko and Mukai*, 2003] model for P_d = 1.8 nPa, IMF B_z = −2.2 nT; pressure-based mapping of THEMIS spacecraft at the end of the growth phase is shown by arrows.

[10] The middle spectrogram in Figure 3 shows the azimuthal pattern of energetic (30–100 keV) proton fluxes plotted against their flow direction in the equatorial plane. During the growth phase it shows a persistent peak centered at +80° and a persistent minimum at a −100° azimuthal angle, which is a known feature usually interpreted as due to the density gradient of energetic particles (increasing earthward or toward the CS center [e.g., *Lee et al.*, 2004]) in the current sheets. Similar anisotropy was observed at P3 throughout the entire growth phase, as well as at P2 and P5 in the first half of growth phase, until they left the plasma sheet. These particle distribution functions at all spacecraft have been successfully reproduced by the 1-D kinetic thin current sheet model in the companion paper by *Zhou et al.* [2010].

[11] The plasma is not homogeneous across the plasma sheet thickness. Before the growth phase electron temperatures varied between 0.25 keV at P2 and 0.6 keV at P4 (Figure 2, bottom). Here and throughout the entire growth phase, T_e varied proportionally to plasma pressure variation (Figure 4, top), which may be understood as spatial variation of the electron temperature along the tail in the plasma sheet central plane. Referring to the empirical model of plasma pressure distribution [*Tsyganenko and Mukai*, 2003], we can connect the observed electron temperatures to the particular distance in the tail as shown in Figure 4 (bottom).

2.2. THEMIS Observations of Substorm Onset

[12] Figure 5 shows a survey of THEMIS observations of substorm onset. Just before onset the magnetic field at P4 was very low (BT <2 nT) with positive B_Z of <~1 nT (at

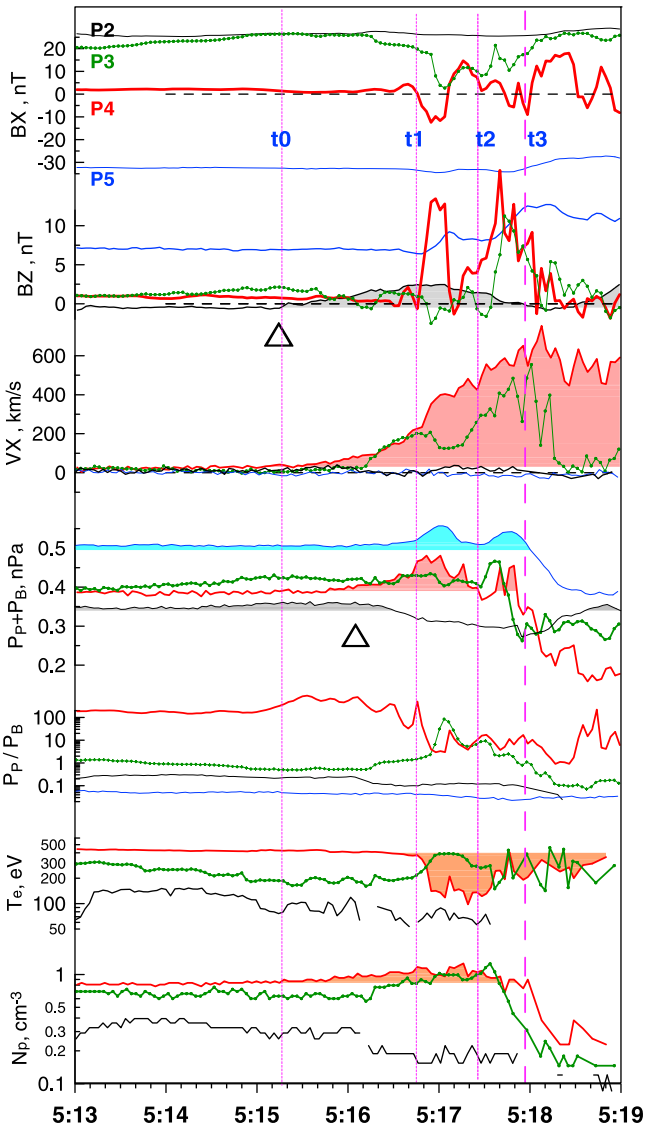

Figure 5. Summary of THEMIS spacecraft observations at substorm onset. Vertical lines indicate the beginning of positive B_z variation at P2 followed by gradual flow and pressure increase at P4 (t_0); two transient dipolarizations and compressions at P4, P5, P3 (t_1, t_2) and intense current disruption associated with the bubble passage (t_3). Start time of current disruption at P2 probe is marked by triangle.

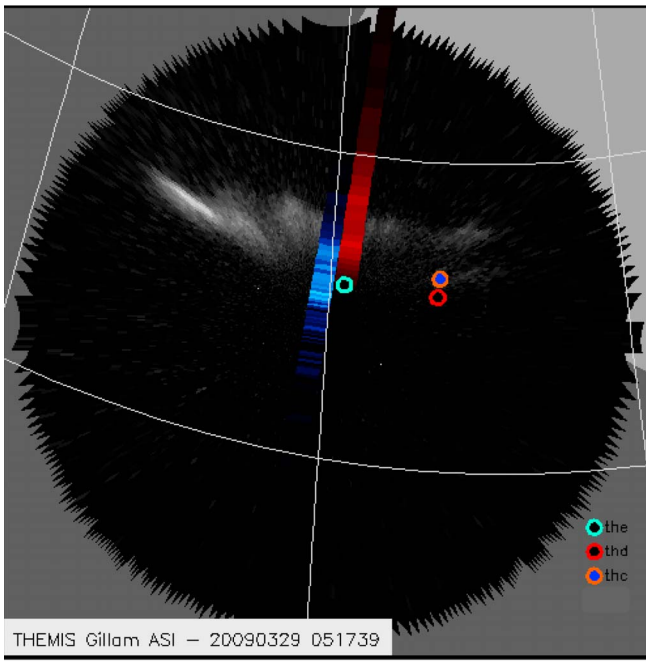

Figure 6. White light ASI image from 051742 which shows the already well-evolved brightening rayed arc, with 630 nm (red line) intensity and H beta (486 nm) intensity from the Gillam MSP overplotted. The ionospheric foot points of THEMIS P2, P3, P4 probes using AM03 model (at 0517:00 UT) are also shown.

about 0515 UT), indicating that this probe remained in the sheet center where the magnetic field shear component and its normal component were both very small. P4 stays at r = 11 R_E in the tail, at the transition between inner dipole-like magnetic field and the thin neutral current sheet.

[13] According to the neutral sheet monitor P4, the onset history looked as follows. The first change signatures appeared gradually after 0515:35 ± 5 s UT, when V_x, density and plasma pressure began to increase gradually. Then a new energetic proton population became visible at azimuthal angles around −20°, coexisting with the previous dawn-dusk anisotropic population, which remained uninterrupted until 0517 UT (Figure 3). This is the first stage of gradual earthward plasma flow/compression at 11 R_E. Sharp intensification of V_x in the middle of this interval was observed at P3 when it entered the inner part of the sheet (see P_p/P_b and B_x variations), indicating that enhanced flow was maximized near the central plane of the plasma sheet.

[14] Sharp change was observed around/after 0516:40 UT (t_1) when B_z increased steeply to 13 nT, accompanied by comparable variations in B_x and B_y components. This occurred simultaneously with an additional V_x increase, disruption of preexisting energetic proton anisotropy pattern, and a surprising drop in T_e from 0.5 to 0.2 keV. Density and total pressure varied but were still enhanced against presubstorm values. This is the second stage with appearance of new plasma, intense transport, transient dipolarization and magnetic field perturbations, and conflicting acceleration signatures (accelerated protons versus cooled electrons; see spectrograms in Figure 3). A second short dipolarization and a flux transport pulse occurred a minute later (t_2).

[15] A sudden drop in plasma density and total plasma pressure, which continued for 3 min, followed since 0517:50 (t_3). During this period the earthward flow varied near its peak values (600 to 800 km/s), and the turbulent magnetic field included a few B_Z enhancements. The proton/electron plasma showed the highest temperatures and largest fluxes at high energies, but the density was reduced four times, causing the largest spacecraft potential of 28 V, more typical of diluted PSBL plasma than of CPS plasma, to be observed (not shown). This third stage corresponds to the arrival of accelerated dilute plasma, which differs from standard plasma bubble only by variable appearance of large B_z field (dipolarization) embedded into the fast flow.

[16] Let us further analyze this episode, taking into consideration observations made by other spacecraft. The earliest indication of substorm onset came from most distant probe, P2 (at X = −14 R_E), which detected positive B_z variation 0515:15 UT (t_0). At that time P2 was in the low-beta outer plasma sheet and did not observe fast flows throughout the entire event. Another important variation was a decrease in B_x and total pressure at P2 that began at 0516 UT, indicating that current disruption process was in progress at 14 R_E distance at the time when the gradual increase in earthward flow and pressure was observed at 11 R_E. The propagation time delay of about 1.5 min between start times of the B_z increase at P2 and P4 is consistent with ~200 km/s earthward flow measured at P4 at the beginning of first transient dipolarization (t_1). At P3 V_x also showed some increase, but the V_x trace was modulated by probe motion into and out of the central plasma sheet. Like P4, P3 also observed a new earthward streaming population of energetic protons, which appeared with maximal counts at a −30° azimuthal angle without interrupting the previous anisotropy pattern. As shown by Zhou et al (this issue) this feature is nicely modeled by the acceleration region (dipolarization front) moving from the tail to 11 R_E.

[17] P5 was just beneath P4 (separated by ~1 R_E in Z, Figure 2), but remained near the plasma sheet boundary (P_p/P_b < 0.1). Comparison reveals similar variations in total pressure at P4 and P5 indicative of approximate vertical pressure balance, with two pressure peaks followed by a final deep pressure drop. Two pressure peaks at P4, P5 are nearly simultaneous with B_z peaks (transient dipolarizations t_1, t_2) at P4, whereas smaller and smoother two-peak B_z variation at P5 is delayed against B_z peaks at P4 by ~10 s. This variation is also recognized at P3 (located 1 R_E dawnward); only the second peak has a large magnitude, however. As discussed in section 3.2, we link the pressure peaks combined with B_z increases with earthward passage of two bulge-like structures in the plasma sheet carrying the reconnected flux tubes.

[18] The final pressure drop observed after 0517:50 UT was very deep, about 50% of preonset values at P4 and P3 located in the PS center, and about 30% at P5 located outside of PS. This indicates decrease in (in that sense, disruption of) the tail current. We note that a smaller total pressure drop started about 1.5 min earlier at P2 located at 14 R_E (~0516 UT, marked by a triangle), suggesting earthward propagation at ~200 km/s velocity. In the lobe (P2 and P5) this drop was weak and smooth.

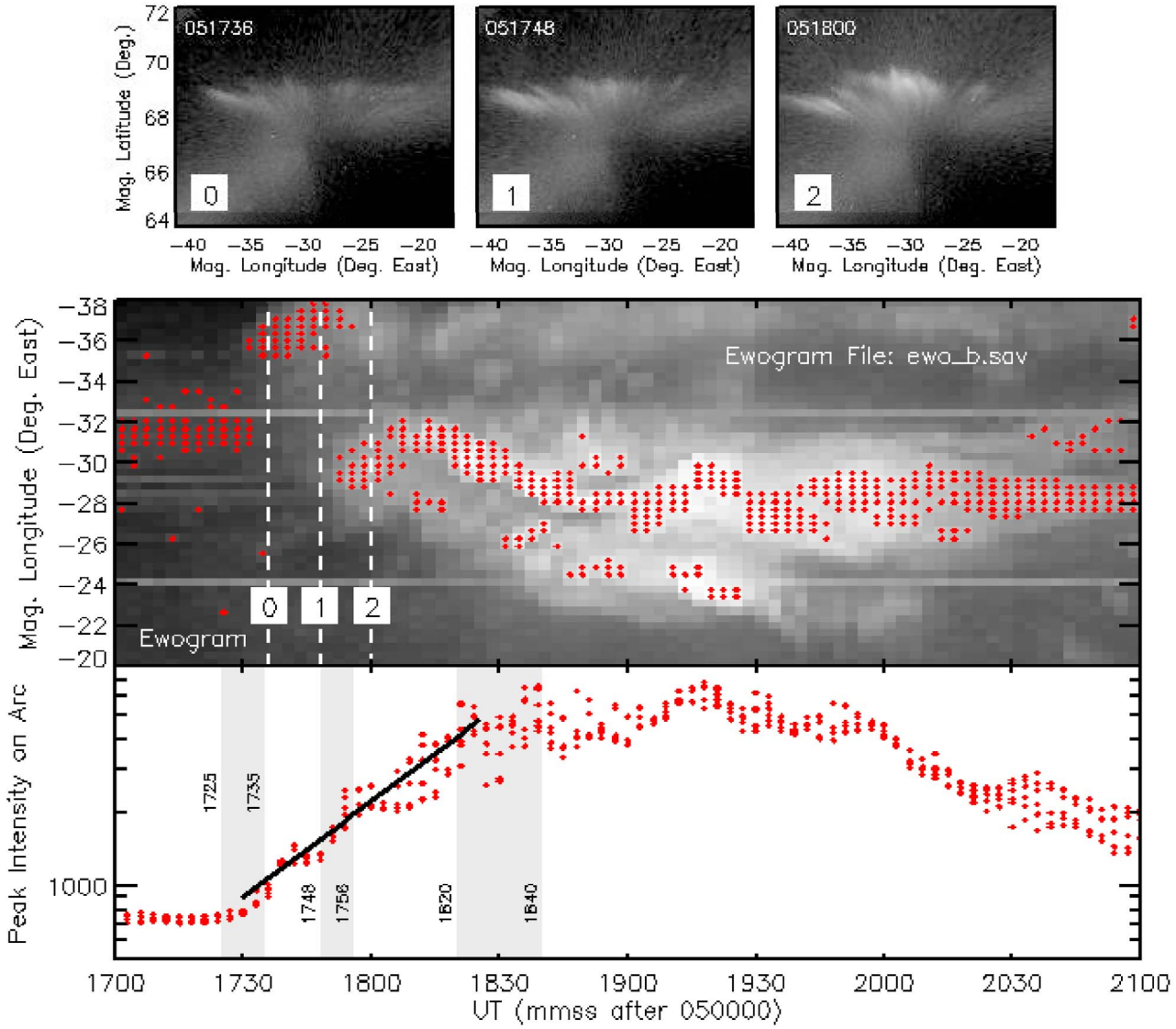

Figure 7. (middle) The Ewogram plotted horizontally. (top) Three auroral images correspond to three times (0,1,2) shown on the EWogram by dashed vertical lines. The red diamonds indicate the brightest six points along the arc (bright locations which represent light contamination are ignored). (bottom) For each longitude, the same six brightnesses that are indicated by the diamonds from the ewogram. The units are pixel count rates ("data numbers"). The solid black line corresponds to exponential growth time t = 30 s.

[19] Whereas no fast flows are observed at P2 and P5 spacecraft in V_x component, both spacecraft show enhanced V_z flows directed toward the plasma sheet center (negative at P2, positive at P5) following B_z variations; they show the inward motion of the plasma tubes after the pressure peak passage.

[20] Although the later stage of expansion phase is not a goal in this paper, we note that dipolarization (positive B_z variation) continue to be turbulent until the fast flow subsides (at 0526 UT at P4), leaving the enhanced B_z (Figure 1). Such a sequence of transient flux transfer concluding with the piled up flux stage (that is, two different types of dipolarizations) is frequently observed in the near tail during substorms [*Nakamura et al.*, 2009].

2.3. Auroral and DMSP Observations

[21] Whereas the main advantage of this study comes from the ideal location and coverage of the THEMIS probes, a second core observation comes from auroral observations, which provide the global context as well as the time and location of the auroral breakup. Auroral onset was observed with a multispectral (λ = 428 (blue), 557 (green), 486 (proton Hβ) and 630 nm (red)) and white light all-sky imager (ASI) at Gillam, Canada. Figure 6 shows the ASI image of a rayed arc soon after the brightening onset with overlapped red line emission and H beta emission distribution along the meridian. The breakup rayed arc is sitting near the poleward boundary of proton aurora and near the equatorward edge of the red emission, that is, in the equa-

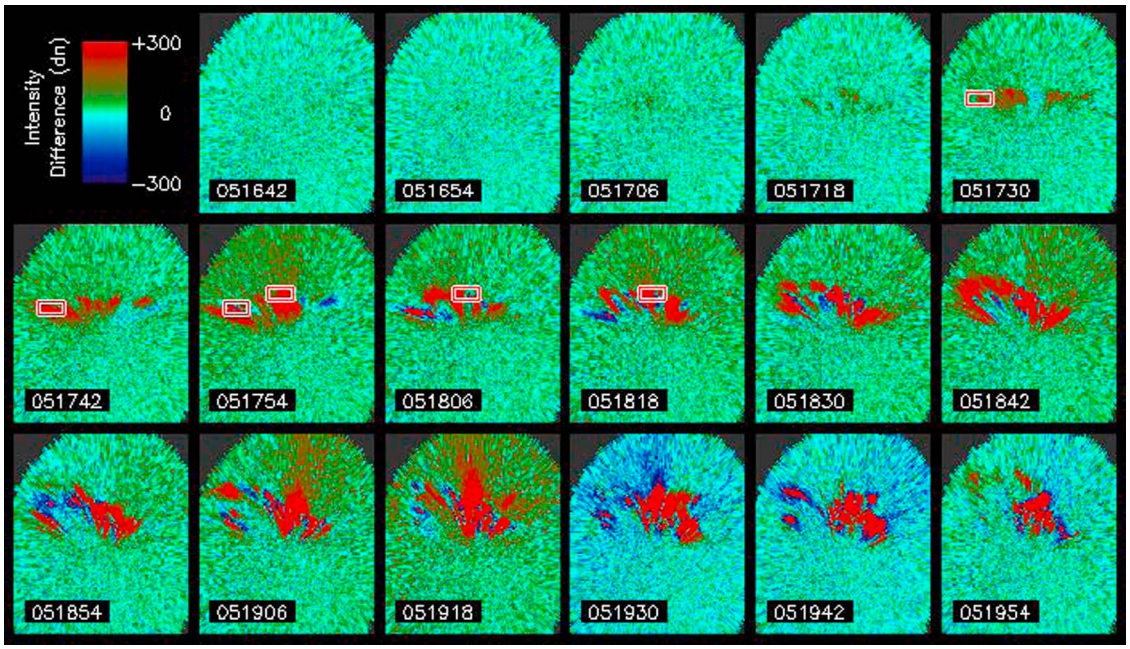

Figure 8. Sequence of difference images spanning the time of initial brightening. Each panel shows the image taken at the time indicated (in hours, minutes, seconds) minus the image taken 12 s previously. The differences are in "data numbers"(dn) with red indicating increasing brightness and blue indicating decreasing brightness (values exceeding plus or minus 300 dn are set to plus or minus 300 dn). The images are plotted in geomagnetic coordinates with east to the right and north up. There are two brightenings separated in longitude by roughly 5°. The first becomes evident at 0517:30 UT, and the second at 0517:54 UT. Both brightenings are indicated by the red and white boxes (each box is shown in three successive frames).

torward portion of plasma sheet precipitation. That the THEMIS probe foot points were mapped with a data-based adapted model (section 2.4) to the central part of Gillam FOV (Figure 6) indicates that measurements in the magnetosphere, especially those at P4, were made near the central meridian of auroral activity. The newly formed rayed arc expanded poleward, and after 0525 UT active auroras were seen in the southern sky of Rankin Inlet situated 6° poleward of Gillam, so the poleward auroral expansion in this event is about 3° in latitude (see keograms in Figure 10 of *Kubyshkina et al.* [2011].

[22] White light observations indicate that initially the auroral event was entirely contained within the Gillam ASI FOV. As shown in the EWogram in Figure 7, brightening began west of Gillam at 58.7° geographic latitude (GGLat) and −99.4° geographic longitude (GGLong) around 0517:30 (first grey band), then died away while starting up near Gillam meridian at the same GG latitude (second grey band). Saturation occurred about a minute after the initial brightening whose maximal intensity along the arc showed exponential growth (with $\tau \sim 30$ s). The well-defined onset of auroral brightening occurred at T_0 = 0517:30 UT ~2° north of Gillam zenith (the coordinates given above and shown in Figure 8 correspond rather to the polewardmost boundary of brightening).

[23] Some activation signatures started earlier, however. For example, the differential images of Figure 8 (means, with previous image subtracted) display some structuring seen at 58.5° starting at about 0517:05 UT. The auroral intensity at this time was decreasing, showing that something was happening in the magnetotail but there was as yet no explosive instability growth. Such different manifestations and timings of auroral breakup are not new; they were discussed by *Donovan et al.* [2008]. An unusual feature of this event is that the prebreakup arc was very faint in the auroral observations at Gillam.

[24] Useful complementary observations come from the DMSP-F17 spacecraft (Figure 9), which crossed the nightside high-latitude portion of the southern auroral oval in the dawn-dusk direction immediately prior to and during initial breakup development. Several minutes before the breakup it crossed the b2i boundary at −66.5° corrected geomagnetic latitutde (CGLat) and ~01 MLT, and then the equatorward edge of diffuse electron precipitation at −66.8° CGLat (comparable to the equatorward limit of red auroral emissions at Gillam, Figure 6). Soon after that it crossed a well-defined inverted V (prebreakup arc?) at −67.5°. After that it traversed the poleward half of the oval at |CGLat| < 70° where it systematically observed cold (100–300 eV), unstructured electron precipitation with some weak proton precipitation embedded. This observation confirms the poleward extent of red emission at ~70° inferred from Gillam observations (e.g., Figure 6) as well as to the cold electron population observed in the outer plasma sheet by THEMIS probes (Figure 4).

[25] Finally, following breakup development, at 0521:45 UT and 21.5 MLT, the spacecraft crossed the wideband (Alfvénic [see *Mende et al.*, 2003]) precipitation (at −68.3°).

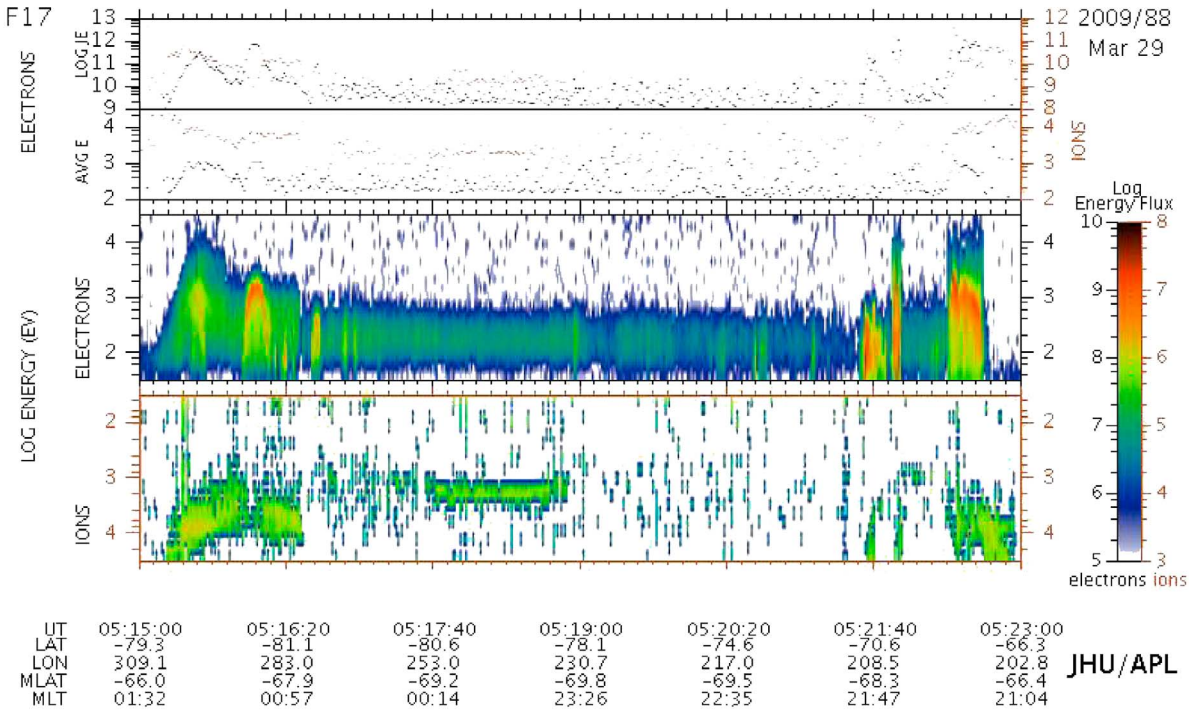

Figure 9. Electron and ion precipitation during the nightside oval crossing in the Southern Hemisphere as observed by SSJ4 instrument onboard DMSP-F17 near the substorm onset time.

Then it crossed above a strong, wide inverted V near −67°, and, after crossing the b2i boundary (−66.6°), traversed into the radiation belt region. DMSP observations together with ground auroral observations confirm that auroral breakup was initiated near the equatorward limit of a moderately wide (3–5°?) auroral oval.

2.4. Modeling and Mapping

[26] A third core constituent in this study is the time-varying, data-based magnetospheric model (for more details, see *Kubyshkina et al.* [2011]). The adaptive model (AM03) includes variable tail and ring currents, additional current sheet tilt, and an additional current sheet of variable thickness to reproduce the thin current sheet. The model was run at a 1 min time step between 0430 and 0530 UT. Magnetic fields observed at THEMIS P2, P3, P4, P5 probes and GOES 12 spacecraft together with total (magnetic + plasma) pressure at P2, have been used as input to the adaptive model. The time variations of observed and modeled fields are compared in Figure 3 of *Kubyshkina et al.* [2011], which shows how much different from observations are the predictions of the standard solar wind-based T96 model and how much better the AM03 adaptive model reproduces the observations.

[27] Figure 10 shows the relationship between northern foot point latitude and outermost (equatorial) distance of the magnetic field lines at the Gillam magnetic meridian (where most THEMIS probes are situated, Figure 2, top), which we later refer to as the "mapping curve." This curve is shown for two epoch times, 0516:00 UT and 0517:00, just around the initial expansion phase features in the plasma sheet and 0–1 min before the breakup, respectively.

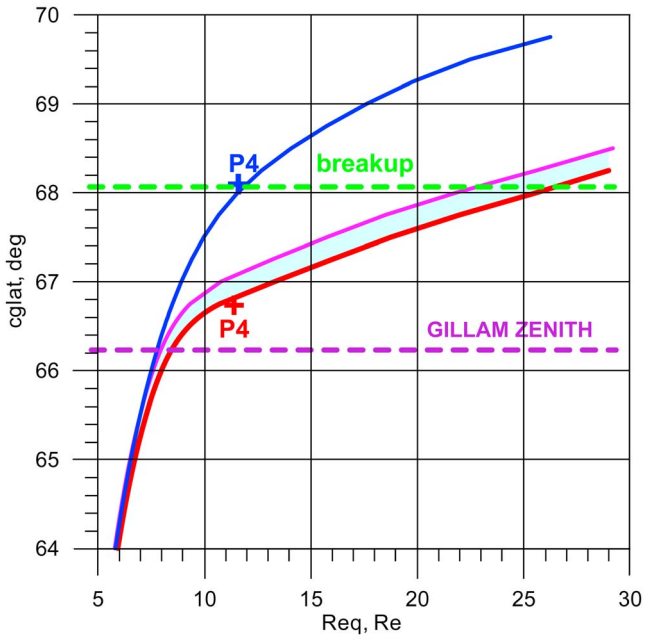

Figure 10. Mapping profile (CGLat versus equatorial distance) at 0516 and 0517 UT on 29 March 2009 (just before the breakup) at 22.5 MLT meridian for adapted AM03 model (red/purple) and for standard T96 model (blue). Corresponding P4 spacecraft mapping are also shown. Gillam zenith (at 110 km) CGLat is shown for reference together with poleward termination of initial breakup arc.

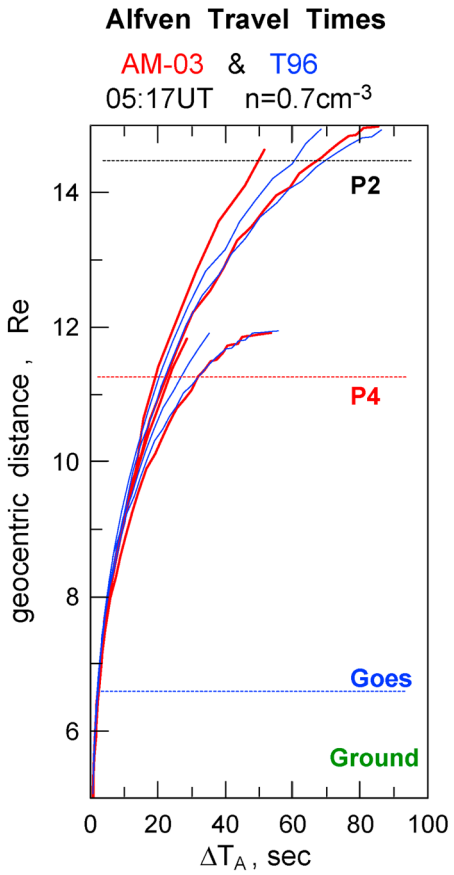

Figure 11. Alfvén time delays computed using T96 (blue) and AM03 (red) models.

The AM03-predicted spacecraft foot points fall well into the region of breakup initiation, about 1.5°–2° latitude poleward of Gillam zenith. The latitudinal width of the flat portion of the mapping curve (where the foot points of the 10–20 R_E equatorial points fall to the ionosphere) is less than 1° latitude. This is comparable to the accuracy of the mapping itself, as estimated from the scatter of foot point coordinates just before the breakup [see *Kubyshkina et al.*, 2011, Figure 9]. Therefore, even with this sophisticated data-based model, the exact equatorial location of the breakup magnetic field line cannot be determined very accurately from mapping. The only thing we may conclude for certain is that the data are consistent with the breakup mapped along magnetic field lines into the thin current sheet, tailward of P4. The mapping curve for the corresponding T96 model and probe locations are also shown for comparison.

[28] In Figure 11 we plot the Alfvén wave travel time from the ground to the magnetosphere using 0.7 cm^{-3}, the density in the central plasma sheet at 11 R_E. The travel time does not show big differences between the standard T96 and adapted models. Four field lines were used for each model. Two cross the neutral sheet at 12 and 15 R_E, and two pass 1 R_E above those equatorial points. Together, these traces characterize a spread of possible time delays to interpret the timing results discussed in section 2.5. Since we ignored the dense ionosphere at low altitudes, the actual time delays can be larger by roughly 10 s than shown in our results (see, e.g., *Lin et al.*'s [2009] calculations).

2.5. THEMIS, Geosynchronous, and Ground-Based Observations

[29] Figure 12 provides a condensed summary of various onset features observed in the thin current sheet at 11 R_E, at geosynchronous spacecraft, and on the ground. The earliest indication of expansion phase onset is the positive B_z variation at P2 (at lobe/plasma sheet boundary) starting at 0515:15 UT, which is soon followed by gradual growth of V_x, plasma density, and pressure at P4. Near this time the earthward streaming ions overlapped onto the dawn-dusk

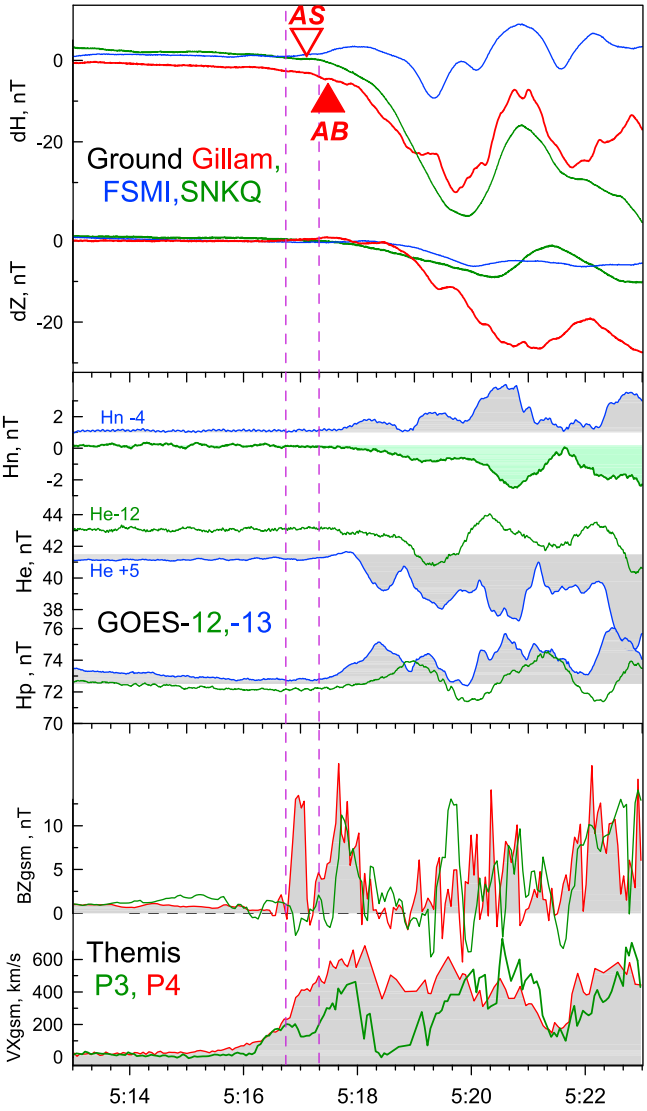

Figure 12. Substorm onset as recorded (from top to the bottom) by ground stations Gillam, FSMI, SNKQ; GOES 12 and GOES 13 spacecraft; and THEMIS P3 and P4 probes. Vertical lines indicate start times of THEMIS dipolarization and of onset-related perturbations at GOES spacecraft. Triangles marked by AS and AB indicate the times of auroral structuring and explosive auroral brightening, respectively.

anisotropy began to be observed. The modeling by *Zhou et al.* [2010] showed that earthward streaming ions are ions that escaped earthward after being accelerated at the earthward moving dipolarization front, so they provide remote sensing of the activity in the more tailward region.

[30] The earliest distinguishable feature at the entry to the dipole-like region (11 R_E) is the sharp dipolarization associated with enhanced flux transport that began at 0516:45 UT. It was observed only by P4 and P5 (B_z variation) not by P3 situated ~1 R_E dawnward from P4, P5; this is consistent with initial brightening at the meridian near and west of the P4 foot point (see Figure 7). The earthward flow had already reached ~200 km/s amplitude by that time. Note that the second dipolarization was observed by both P3 and P4, in agreement with eastward expansion of active auroras (Figure 7).

[31] In this event GOES 12 and GOES 13 spacecraft bracketed the breakup meridian and THEMIS constellation from east and west, respectively (see Figure 2, top). After onset they both observed positive variations in the H_p (north) component, negative variations in the earthward H_e component, and variations of opposite sign in the H_n (east component), consistent with substorm current wedge effects [*Nagai*, 1982]. The variations were deeply modulated by the Pi2 signal with an apparent period of about 1 min. The gradual changes began at 0517:00 UT, with clearer changes visible after 0517:20 UT. The Alfvénic time delay of 15–30 s from 11 R_E to 6.6 R_E (Figure 11) is consistent with these observed delays.

[32] Ground magnetometer data from Gillam and two more stations (FSMI and SNKQ) with similar CGLat but displaced in MLT by ~1 h to the west and east (respectively) displayed negative H component bays and a negative Z component bay at Gillam (reflecting the poleward expansion of the electrojet). The magnitude of variations was only 30 nT. In addition, the midlatitude stations recorded very clear midlatitude bays in H and D components strongly modulated at the Pi2 frequency, the pattern of which corresponds closely to the classical SCW located in the MLT sector between 20 and 24 MLT (not shown). According to all these data, the gradual magnetic perturbations started not earlier than at 0517:00 UT, with clearer changes visible after 0517:15–0517:20 UT. As described in section 2.3, the explosive auroral brightening (AB) over Gillam started at 0517:30 UT, with weak signatures of auroral structuring evident from 0517:05 UT (AS) onward. Although the very brief Alfvénic time delay from 6.6 R_E to the ionosphere (Figure 11) does not contradict the observations, gradual onsets preclude us from making a more detailed discussion.

[33] In conclusion, we found (1) earthward progression of onset from 14 R_E to 11 R_E and to geosynchronous orbit; (2) relatively long time delay between signatures at 14 R_E and at 11 R_E (about 90 s, clearly larger than local Alfvénic transport time); (3) much shorter delay between 11 R_E and 6.6 R_E; and (4) nearly simultaneous onset on geosynchronous orbit and the ionosphere.

3. Discussion

3.1. The 29 March 2009 Substorm as a Generic Event

[34] Here we would like to emphasize that the characteristics of this event are typical; with a very few question marks (e.g., is it substorm or pseudobreakup?), it can be regarded as a generic substorm. Its general picture looks very familiar, consistent with definition given in the Introduction. It started after quiet period with northern IMF, after the IMF southward turning. In the magnetotail the growth phase continued for ~50 min and included such well-known manifestations as the H component depression (~10 nT) at the nightside portion of geostationary orbit, the growth of the tail lobe field and of total current in the near-Earth magnetotail (by ~12% and ~1 MA), earthward motion of intensified tail current (by ~1 R_E [see *Kubyshkina et al.*, 2011, Figure 6]), and overall stretching of magnetic configuration quantified by time-dependent data-adaptive model. At the concluding stage of the growth phase, a thin current sheet (TCS, thinning below the 0.15 R_E upper estimate as given by the Harris half thickness scale, Figure 2) was embedded in the near-Earth plasma sheet. The last 10–15 min of the growth phase appeared to be a time of explosive TCS growth. During this time, the entire plasma sheet was also thinning; its half thickness at $r \sim 11$ R_E decreased below 1 R_E so that P5 exits almost to the lobe. These manifestations are well-known features of the substorm picture in the magnetotail first outlined by *McPherron et al.* [1973] and later developed and complemented by many authors [see, e.g., *Nishida and Hones*, 1974; *Caan et al.*, 1978; *Forbes et al.*, 1981; *Lui et al.*, 1992; *Sanny et al.*, 1994; *Baker et al.*, 1996; *Sergeev et al.*, 1993, 2005; *Nagai et al.*, 1998; *Shiokawa et al.*, 1998; *Angelopoulos et al.*, 2008; *Miyashita et al.*, 2009; *Petrukovich et al.*, 2007, 2009]. Our study allows us to quantitatively characterize various manifestations in the same event.

[35] The physics of the growth phase reconfiguration is generally linked to the combination of two factors: enhanced tailward transport of magnetic flux tubes reconnected on the dayside magnetopause and low earthward transport rate (back to the dayside) in the plasma sheet. The latter factor, which in some theories is explained by specific thermodynamic properties of the magnetotail ("pressure balance inconsistency" [see, e.g., *Wolf et al.*, 2009]), is not quantitatively well known from observations. Here, for the first time, we provide the transport rate as measured in the neutral sheet at the entry to the dipole-like inner region during the entire 50 min long growth phase. The average value of $[BV_i]_y \sim 0.01$ mV/m appeared to be ~10–20 times lower than the expected balanced flux transfer ~ 0.15 mV/m (estimated as the 50 kV cross-tail potential divided by the tail diameter 50 R_E). Therefore, the earthward flux transfer was strongly suppressed at the nightside in the region in which the thin current sheet formed. This estimate is more accurate than estimates made outside the neutral sheet, which suffer from the contribution of north-south (thinning and flapping) flux tube motions and V_z component offsets.

[36] Expansion phase operational signatures (auroral breakup and subsequent poleward expansion, explosive growth of the westward electrojet and substorm current wedge, Pi2 pulsations) are also quite standard, although at low intensity. Onset signatures in the near-Earth magnetotail (current disruption, earthward plasma injection, dipolarization and expansion of the plasma sheet) are also standard [see, e.g., *McPherron et al.*, 1973; *Lui et al.*, 1992; *Sergeev et al.*, 2005; *Angelopoulos et al.*, 2008]. The same is true concerning the auroral breakup morphology (section 2.3).

The breakup began as structuring of auroras, followed by an exponential growth in auroral brightness with an *e*-folding time of ~30 s [*Liang et al*., 2008; *Donovan et al.*, 2008]. As usual, our breakup began near the equatorward edge of the auroral oval [*Akasofu*, 1964], near the equatorward limit of red emission, and at the poleward slope of proton-induced 486 nm emission [*Samson et al.*, 1992].

[37] Concluding this section, we recall that all critical manifestations of the studied event are generic, so the physics of this event must also be very general. The intensities of principal changes in the near-Earth tail, such as the amount of energy storage, explosive growth of embedded TCS, explosive dissipation in the current sheet during the expansion phase (E_y bursts up to 5–10 mV/m), bursty flows, and plasma bubbles, are typical of modest substorm events. The only difference is that near-Earth signatures of 3-D substorm current system were rather weak: SCW of ~0.1 MA (estimated from midlatitude magnetograms), GOES and midlatitude magnetic bays of a few nT intensity, and especially the auroral zone bays which were below 50 nT during first 10 min of the expansion phase.

[38] A weak ground magnetic effect may not necessarily be connected to a small intensity of 3d currents in the magnetotail. In fact it can be explained by the cold/dense state of the plasma sheet (density about 0.8 cm^{-3}, T_i < 3 keV, T_e < 0.5 keV) prior to substorm onset. As previously discussed by *Yahnin et al.* [2001] and confirmed in the ground-tail correlative study by *Sergeev et al.* [2004], according to the Knight relationship, the cold/dense plasma sheet has more electric current carriers and requires less field-aligned acceleration to keep the field-aligned current (FAC) current at the same intensity as generated by magnetospheric process, than does the less dense, hotter plasma sheet. Weak acceleration severely decreases hard electron precipitation and Hall conductivity, which, in turn (applying the Fukushima theorem), results in strongly suppressed ground magnetic perturbations (though R1/R2 current systems and Pedersen currents can still be quite intense). This means that the dissipative processes may be quite strong in the plasma sheet, whereas their image in ground magnetic perturbations is weak in that particular (cold/dense) state of the plasma sheet.

[39] In some previous studies short substorm-like magnetospheric events showing a weak ground magnetic effect were separated from substorms and called as pseudobreakups (PBUs) (see *Kullen and Karlsson* [2004] for a summary of recent and previous work). A distinctive feature suggested for PBUs was that they have no macroscopic consequence, that they do not develop into the full-scale substorm. This is not supported by modeling result that during 10 min long expansion phase (0517–0526 UT) the total plasma sheet current between 5 and 20 R_E decreased by ~1 MA, or by 25% [*Kubyshkina et al.*, 2011]. This value is comparable to the entire tail current increase during preceding 45 min long growth phase. Also magnetospheric and auroral configuration changed considerably during expansion phase resulting in the poleward shift of spacecraft ionospheric foot points by ~3–4° CGLat as well as in the poleward auroral expansion of the similar magnitude. Therefore, whereas this is a matter of taste to select one or another name (PBU or substorm) in the absence of strict quantitative definition of each term, a short expansive phase in this case has quite global consequences in terms of total current, configuration changes and auroral expansion.

3.2. Interpretation of THEMIS Observations at 11 R_E: Indirect Evidence of Magnetic Reconnection

[40] A number of new, interesting observations shed some light on the origin of substorm onset process. The first concerns onset-related transient dipolarizations in the thin current sheet, which are simultaneously observed by two closely spaced but vertically separated probes, one (P4) near the neutral sheet and another (P5) in the adjacent lobe. During initial activity P4 recorded two strong pulses of B_Z embedded into the fast flows. They were accompanied by two pulses of total pressure (times t_1 and t_2 in Figure 5), followed by a deep pressure drop (starting at t_3). Very similar B_Z and total pressure variations (although of low magnitude) were also recorded at P5, which was that time almost in the lobes (P_p/P_b < 0.1). Figures 13e–13i show these variations in the expanded scale and in the normalized form. It is convenient to compare them with the predictions of transient reconnection theory. A recent review paper by *Sharma et al.* [2008, Figure 30] provides a convenient illustration to compare with our observations; it is shown in Figures 13a–13d. In the model the two-pulse reconnection rate (E*, Figure 13b) in the thin current sheet separating antiparallel magnetic fields (with B_z = 0) was set up at the reconnection line at X = 0. These pulses formed a two-hump reconnection exhaust structure containing reconnected flux tubes frozen into the heated fast flowing plasma, as shown schematically in Figure 13a. The reconnection exhaust propagates outward at the Alfvén velocity in the reconnection inflow region, and its Z size grows proportionally to the distance (X) from the reconnection line (Figure 13a). The lobe magnetic variations produced at four virtual spacecraft (points a–d in Figure 13a) are shown in Figures 13 and 13d. Here all variations are normalized on the initial lobe field value (which is also subtracted from the B_x component variation; see *Sharma et al.* [2008] for more details).

[41] To compare with observations, we emphasize the variations at point d, which remained close to the neutral sheet and at considerable distance from the reconnection line, as P5 probably did. The normalized B_x and B_z variations observed at P5 (Figures 13e and 13f) have amplitude and shape similar to those predicted at point d. They display 2 min scale B_X humps followed by B_X drop below its initial value, which is a signature of current disruption or, in other words, of loss of reconnected magnetic flux from the lobe. In the model two B_X humps (two lobe field compressions) are produced by two exhaust bulges passing nearby (Figure 13a). They are accompanied by asymmetric bipolar B_z variation with predominant positive B_Z (initial weak negative pulse is clearly seen only for the first exhaust bulge). The phase of B_Z variation is delayed by a quarter of period against B_X positive variation, which is also consistent with observations.

[42] The transient reconnection model also predicts a good correlation of δB_z with up/down flux tube motions ($\delta B_z \sim +\delta V_z$ for the southern lobe), which is also nicely observed at P5 (compare Figures 13f and 13g). Numerically a linear regression between these variables is δB_z [nT] = $0.05\delta V_z$ [km/s] (correlation coefficient CC = 0.90), it corresponds to Walen (Alfvén wave) relationship for

effective density ~ 1 cm^{-3}. Last but very important, in the model, B_X compressions are nearly collocated with localized enhanced magnetic flux closures (B_Z pulses) across the current sheet center plane (Figure 13a). This is exactly what we see at P4 near the neutral sheet in our case. In summary, the comparison of observations with model predictions demonstrates good agreement in all essential points and provides strong support to the reconnection origin of the magnetic field variations observed at the substorm onset at 11 R_E, near the earthward edge of the neutral thin current sheet.

[43] Initially, reconnection proceeds deep inside the closed plasma tubes, however, where the magnetic field is relatively small and density in the reconnection inflow region is higher than in the lobes. This explains the relatively small flow velocities in the BBF (a few hundred kilometers per second) and relatively large initial propagation time delay between current disruption signatures, about 1.5–2 min between 14.5 and 11 R_E. Such delays are consistent with the simple Alfvénic time delay calculations displayed in Figure 12.

[44] An unusual feature of the observations is an obvious delay in bubble arrival as evidenced by the deep density and plasma pressure drop at P3, P4 beginning at time t_3, 0517:50 UT ± 10 s), a minute after transient dipolarization. This looks different from ordinary plasma sheet BBFs in which a sharp B_z increase coincides with a sharp density drop;, see, e.g., statistics of *Ohtani et al.* [2004] and multi-spacecraft observations of *Runov et al.* [2009]. We explain this by different generation conditions; namely, that in our event reconnection initially proceeded on closed field lines, whereas it acted on lobe field lines in the majority of other BBF observations. In closed flux tube reconnection, the density/pressure in reconnecting tubes is relatively large; the bubble features (including entropy drop and electric polarization) are less expressed; and 2-D-like interaction of flow with ambient plasma (compression) is stronger than in lobe reconnection. As time proceeds the less dense plasma tubes start to be reconnected and finally the bubble features may dominate in the BBF over the compression effects. Such a scenario with onset initiation on closed field lines is supported by auroral observations (Figure 6 and section 2).

[45] During this initial "BBF+dipolarization without bubble" stage, a remarkable variation in electron temperature was also observed in the neutral sheet: during the first transient dipolarization (at t_1 time in Figure 5, see also color plots in Figure 3), T_e dropped sharply by a factor of 2.5 (from 0.5 to 0.2 keV) and stayed at that level for about a minute. This occurs in the earthward moving plasma tube in which the proton temperature and high-energy flux both increased concurrently with a small increase in the plasma density. Any explanation of these facts should require that (1) the temperature of electrons in the source plasma tube is initially much lower than T_e values at 11 R_E in the neutral sheet, and that (2) the effectivity of acceleration is not large

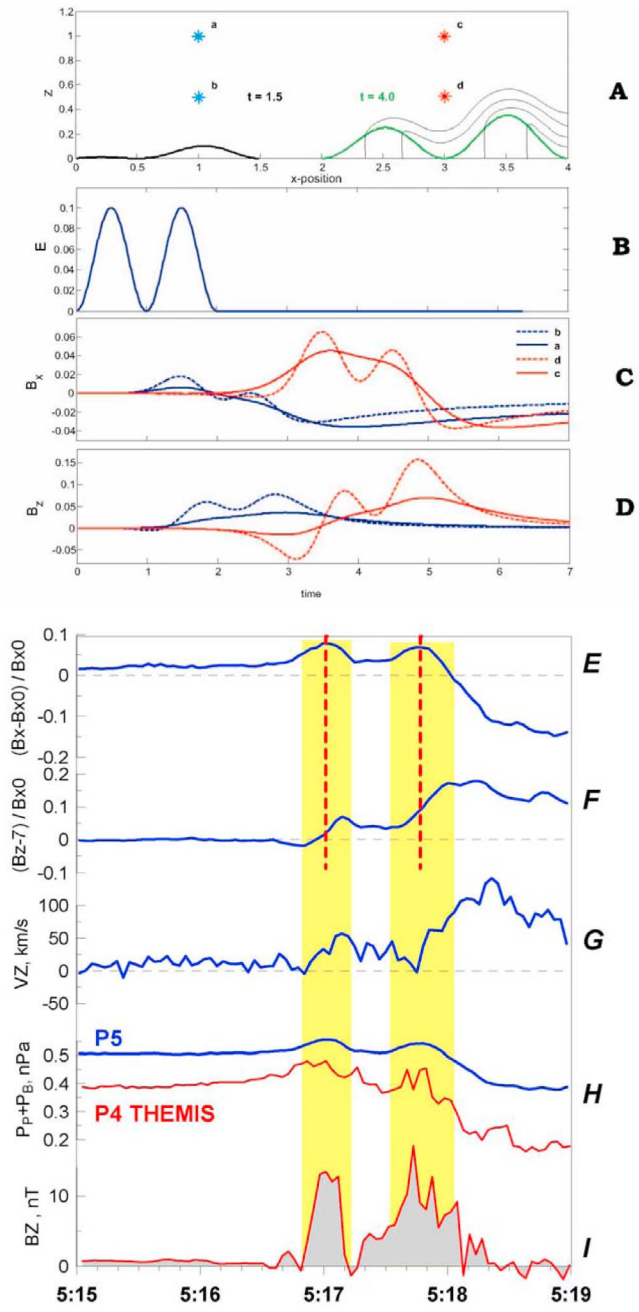

Figure 13. Predictions of transient reconnection model for the case of two consequent reconnection pulses (adapted from [*Sharma et al.*, 2008, Figure 30]). (a) Configuration of upper halves of reconnection outflows in *XZ* plane at two instants of time (t = 1.5 and t = 4.0), reconnected magnetic field lines threading the outflow bulges are also shown by grey lines; (b) time variations of reconnection rate E*; (c and d) variations of $\delta B_x (B_x = 1 + \delta B_x)$ and B_z magnetic field components predicted at four points (a, b, c, and d) above the current sheet whose location is shown in Figure 13a. All quantities are normalized (see *Sharma et al.* [2008] for more details). Vertical dotted lines in Figures 13e and 13f facilitate to observe the phase shifts between variations in B_x and B_z components. (e and f) Variations of magnetic field and (g) of V_z plasma flow at THEMIS P5 probe; (h) total pressures at P4, P5 probes; and (i) B_z component variations in the neutral sheet. Shading indicates two episodes of strong magnetic flux closure through the neutral sheet region which have associated TCR-like variations in the lobe.

and is different for protons and electrons. An explanation of the low electron temperature is very important. It seems impossible to reproduce this effect by suggesting the inner magnetosphere as a source (because plasma is hotter in the inner plasma sheet), so it shows a great preference for the tailward source.

[46] The reconnection mechanism together with the observed strong radial gradient of electron temperature (Figure 4) provide a better explanation for the requirement (1), because the external (colder) plasma tubes are involved in this process. Based on Figure 4 one concludes that the reconnection should initially cut (reconnect) the field lines that cross the neutral sheet at $r > 20$–$25\ R_E$ where the electrons have the required $T_e < 0.2$ keV. As regards requirement (2), its explanation can include a combination of mechanisms, like different acceleration efficiency of various species (e.g., nonadiabatic protons at Speiser orbits versus adiabatic electrons), the azimuthal dependence (longitudinal effects due to P4 location near the flank of the acceleration region and BBF), etc. These kinetic aspects are as yet very little studied and remain a subject for special study. In any case the observed effect points toward the tailward plasma source, which has the required cool population and is transported in the earthward direction in agreement with observations.

[47] The more distant tail (beyond 15 R_E) was not directly probed in our event. Nevertheless, we can infer the location of reconnection at distances between about 15 and 20 R_E by combining various observations, including the following: (1) the positive sign of B_z variation at P2 (which is also the earliest of all onset signatures) points to $r > 15\ R_E$, (2) the similarity of B waveforms observed at P5 (at $dZ_{ns} \sim 1\ R_E$) with variations predicted for virtual spacecraft d in Figure 13 indicates that the reconnection distance may be comparable to 6 R_E; therefore, $r \sim 17\ R_E$, (3) *Zhou et al.* [2010] reproduced the proton distribution functions prior to dipolarization arrival at P4 with a simple model including an earthward propagating dipolarization front, and they concluded that the observed time delay of the first appearance of the earthward streaming population superimposed onto the previous dawn-dusk pattern is consistent with $r \sim 15\ R_E$ (up to 20 R_E), and (4) breakup mapping using the AM03 model at 0517 UT is consistent with the breakup source earthward of 25 R_E (Figure 10) [see also *Kubyshkina et al.*, 2011].

[48] Recently, *Miyashita et al.* [2009] published a Geotail survey of magnetotail effects ordered by auroral breakup (for a few thousand events), and *Petrukovich et al.* [2009] published a survey of 49 Cluster observations made at substorm onset near the thin current sheet. Both groups concluded that the most probable location of reconnection at substorm onset is around 17–18 R_E, with the possibility of much more earthward reconnection in the premidnight MLT sector [*Petrukovich et al.*, 2009]. The inferred range of initial reconnection locations (15–20 R_E in our case) is therefore nicely consistent with the most systematic, comprehensive statistical surveys available so far.

3.3. Toward a Unified Interpretation of Onset Observations

[49] Lack of key observations has led to debates concerning source region location and substorm instability and auroral breakup generation. Not pretending to review these problems in detail and to give final answers (which probably requires a full-scope review volume), here we briefly summarize what new constraints our "ideal configuration" (covering both neutral sheet and lobe at the junction between the inner region and TCS, conjugate to breakup) brings to this discussion.

3.3.1. Breakup Location and Mapping

[50] Auroral breakup develops near the equatorward border of the auroral oval, at the equatorwardmost arc and within a region of proton precipitation [*Akasofu*, 1964; *Samson et al.*, 1992; *Donovan et al.*, 2008; *Lyons et al.*, 2002; *Rae et al.*, 2009]. Using the accurate magnetospheric model, we confirm the standard interpretation (that the breakup is initiated deep inside the closed flux tube plasma sheet region). Another conclusion usually drawn after mapping such a location into the magnetosphere (first discussed by *Samson et al.* [1992] and *Elphinstone et al.* [1991]) is that the breakup initiates deep inside the dipole-like region (e.g., T96 mapping curve, Figure 10). Mapping using the standard model is inaccurate for mapping purposes, however. Actual mapping, as shown by AM03 model results, is very different. When the AM03 model is used, the breakup area is mapped further into the tail rather than into the dipole-like region; this is consistent with the 15–20 R_E reconnection location inferred in section 3.2. For more discussion, see *Kubyshkina et al.* [2011].

3.3.2. Rarefaction Wave

[51] The scenario of turbulent current disruption [e.g., *Lui*, 1996] suggests that current disruption in the dipole-like inner region can launch a tailward propagating rarefaction wave that sucks the plasma in. Therefore, the total pressure decrease should initiate the earthward plasma flow. This is opposite to what is observed: both the plasma pressure at the neutral sheet (at P4) and the magnetic pressure in the lobe (at P5) grew together with gradually increasing earthward flow after 0515:40 UT (and continued to increase at the beginning of the BBF), indicating that they are associated with plasma pumping in, rather than with the rarefaction wave. The compression can be understand as a partial plasma pileup in front of the earthward propagating dipolarization front coming from the midtail (see below). According to surveys by *Xing et al.* [2010] and *Dubyagin et al.* [2010], compression-associated earthward flow onsets are common at distances $\leq 12\ R_E$ at substorm onset. Therefore, observational evidence negates the rarefaction wave hypothesis.

3.3.3. Tailward Propagating Current Disruption

[52] Interpretation of lobe observations made at 15–20 R_E in a few events [*Jacquey et al.*, 1991; *Ohtani et al.*, 1992] is frequently cited as evidence for a near-Earth location of current disruption. The authors of these studies inferred the initial location of current disruption to be at $r < \sim 10\ R_E$, with subsequent tailward propagation of current disruption. The method is, of course, not very precise concerning the initial location of current disruption because the model used (a slab of dawn-dusk current) is too simple and the spacecraft is too far from the inferred onset location. Moreover, a near-Earth location of reconnection was inferred based on initial negative B_z variation, which may have very different origins. For example, in Figure 13d, the negative dB_z in the lobe is formed at virtual spacecraft c and, especially, d sitting on the

earthward side of the X line reconnection. Therefore, this evidence is not conclusive as concerns the initial location of the current disruption.

3.3.4. Synergy in the Description of Plasma Sheet Variations Around Substorm Onset

[53] A number of different transient plasma structures have been suggested in the literature; many of them can be recognized in our data within a few minutes of substorm onset. Certainly, BBFs and bubbles are among them. Also, B_x compressions with associated B_z variations in Figure 13 resemble the traveling convection regions (earthward TCRs) [*Slavin et al.*, 2005], previously linked to earthward motion of magnetic islands or flux ropes). Lobe B_x variations also show a drop and share many similar features with variations interpreted as propagating current disruption (CDs) [*Jacquey et al.*, 1991; *Ohtani et al.*, 1992]. Finally, nightside flux transfer events (NFTEs) [*Sergeev et al.*, 1992] have properties and interpretation similar to what has been described in section 3.2 (propagation of reconnection outflow bulges generated by transient reconnection). Our analysis allows us to argue that a variety of onset-related magnetotail phenomena discussed in the past literature under the different names (BBFs, bubbles, current disruption, NFTEs, earthward TCRs) are due to the same dissipative structure (reconnection outflow bulge) observed from different vantage points.

[54] At this point we would like to emphasize that a simple time-varying reconnection model [*Semenov et al.*, 2005] produces the waveforms in the lobes (Figures 13c and 13d), which are strongly position dependent. The two hump TCRs formed by two reconnection pulses are resolved only by an observer sitting near the lobe-PS boundary (at points b,d) and are smeared out in points a, c whose distance is larger than the separation between the two bulges in X. Positive dB_x variations (TCRs) are well resolved only if the X distance and Z/X distance ratios are both large (in point d). Only the $|B_x|$ drop and positive B_z excursion are observed robustly at all points. This implies that interpretation of lobe magnetic variations requires a careful analysis using an inverse problem solution and incorporating a priori information. For more details, see, e.g., *Semenov et al.* [2005] and *Kiehas et al.* [2009].

4. Conclusions

[55] Taking advantage of the ideal coverage of THEMIS and GOES spacecraft, we were able to characterize quantitatively configurational changes in the near-Earth nightside magnetotail during the substorm event on 29 March 2009. These include the growth of tailward stretching under the suppressed earthward convection in the nightside plasma sheet (reduced to <10% of expected balanced flux transfer rate), explosive growth of the thin current sheet at around 10–12 R_E (down to Harris half thickness of 0.15 R_E) and associated severe local thinning of the plasma sheet during the concluding 10–15 min of the growth phase. Altogether these changes produced a peculiar configuration with a sharp junction of the dipole-like region with the quasi-neutral thin current sheet at around 11 R_E, where the magnetic field was very small ($B_z < 1$ nT).

[56] Four THEMIS probes observed this junction in the neutral sheet and adjacent lobe at substorm onset in the region conjugate to the breakup, that is, in ideal locations to resolve controversies related to substorm onset physics. All types of data analysis (neutral sheet and lobe observations, timing, magnetic field mapping using data-adapted model, DF modeling, etc.) consistently point to the same source location of auroral breakup and of plasma sheet earthward flux transfer, which are both initiated in the thin current sheet, most probably between 15 and 20 R_E in this event. The observations definitely exclude the rarefaction wave propagating from the inner region as the BBF source. Having analyzed the lobe waveforms and inferred their reconnection origin, we argue that different onset-related magnetotail phenomena discussed in the past literature (BBFs, bubbles, current disruption, NFTEs, earthward TCRs) are the views of the same dissipative structure formed by reconnection, observed from different vantage points. Altogether this event provides a synergistic description of basic configurational and plasma changes and provides a definite choice against the breakup initiation on dipole-like field lines and in favor of reconnection in the thin current sheet as basic substorm onset process.

[57] **Acknowledgments.** Data from the SSJ4 particle spectrometer (D. A. Hardy PI) on board the DMSP F-17 have been made available via JHUAPL Web site, the OMNI database is run by the NGDC at NASA Goddard Space Flight Center. We thank all data providers for their valuable data sets. Thanks to K. H. Glassmeier, U. Auster, and W. Baumjohann for the use of FGM data provided under the lead of the Technical University of Braunschweig and with financial support through the German Ministry for Economy and Technology and the German Center for Aviation and Space (DLR) under contract 50 OC 0302. We thank A. Nikolaev and S. Apatenkov for their help in data processing, M. Kholeva and Judy Hohl for help in preparing the manuscript. The work was supported by THEMIS contract NAS5-02099. The work by V.S. and M.K. was also supported by Russian Ministry of Science grants and by RFBR grants 10-05-91163 and 10-05-00223.

[58] Masaki Fujimoto thanks the reviewers for their assistance in evaluating this paper.

References

Akasofu, S.-I. (1964), The development of the auroral substorm, *Planet. Space Sci.*, *12*, 273–282, doi:10.1016/0032-0633(64)90151-5.

Angelopoulos, V., et al. (2008), Tail reconnection triggering substorm onset, *Science*, *321*, 931–935, doi:10.1126/science.1160495.

Baker, D. N., T. I. Pulkkinen, V. Angelopoulos, W. Baumjohann, and R. L. McPherron (1996), The neutral line model of substorms: Past results and present view, *J. Geophys. Res.*, *101*, 12,975–13,010, doi:10.1029/95JA03753.

Caan, M. N., R. L. McPherron, and C. T. Russell (1978), The statistical magnetic signature of the magnetospheric substorms, *Planet. Space Sci.*, *26*, 269–279, doi:10.1016/0032-0633(78)90092-2.

Donovan, E., et al. (2008), Simultaneous THEMIS in situ and auroral observations of a small substorm, *Geophys. Res. Lett.*, *35*, L17S18, doi:10.1029/2008GL033794.

Dubyagin, S., V. Sergeev, S. Apatenkov, V. Angelopoulos, R. Nakamura, J. McFadden, D. Larson, and J. Bonnell (2010), Pressure and entropy changes in the flow-braking region during magnetic field dipolarization, *J. Geophys. Res.*, *115*, A10225, doi:10.1029/2010JA015625.

Elphinstone, R. D., D. Hearn, J. S. Murphree, and L. L. Cogger (1991), Mapping using the Tsyganenko long magnetospheric model and its relationship to Viking auroral images, *J. Geophys. Res.*, *96*(A2), 1467-1480, doi:10.1029/90JA01625.

Forbes, T. G., E. W. Hones Jr., S. J. Bame, J. R. Asbridge, G. Paschmann, N. Sckopke, and C. T. Russell (1981), Substorm-related plasma sheet motions as determined from differential timing of plasma changes at the ISEE satellites, *J. Geophys. Res.*, *86*(A5), 3459–3469, doi:10.1029/JA086iA05p03459.

Jacquey, C., J. A. Sauvaud, and J. Dandouras (1991), Location and propagation of the magnetotail current disruption during substorm expansion: Analysis and simulation of an ISEE multi-onset event, *Geophys. Res. Lett.*, *18*(3), 389–392, doi:10.1029/90GL02789.

Kiehas, S. A., et al. (2009), First application of a Petschek-type reconnection model with time-varying reconnection rate to THEMIS observations, *J. Geophys. Res.*, *114*, A00C20, doi:10.1029/2008JA013528.

Kubyshkina, M., V. Sergeev, N. Tsyganenko, V. Angelopoulos, A. Runov, H. Singer, K. H. Glassmeier, H. U. Auster, and W. Baumjohann (2009), Toward adapted time-dependent magnetospheric models: A simple approach based on tuning the standard model, *J. Geophys. Res.*, *114*, A00C21, doi:10.1029/2008JA013547.

Kubyshkina, M., V. Sergeev, N. Tsyganenko, V. Angelopoulos, A. Runov, E. Donovan, H. Singer, U. Auster, and W. Baumjohann (2011), Time-dependent magnetospheric configuration and breakup mapping during a substorm, *J. Geophys. Res.*, doi:10.1029/2010JA015882, in press.

Kullen, A., and T. Karlsson (2004), On the relation between solar wind, pseudobreakups, and substorms, *J. Geophys. Res.*, *109*, A12218, doi:10.1029/2004JA010488.

Lee, E., M. Wilber, G. K. Parks, K. W. Min, and D.-Y. Lee (2004), Modeling of remote sensing of thin current sheet, *Geophys. Res. Lett.*, *31*, L21806, doi:10.1029/2004GL020331.

Liang, J., E. F. Donovan, W. W. Liu, B. Jackel, M. Syrjäsuo, S. B. Mende, H. U. Frey, V. Angelopoulos, and M. Connors (2008), Intensification of preexisting auroral arc at substorm expansion phase onset: Wave-like disruption during the first tens of seconds, *Geophys. Res. Lett.*, *35*, L17S19, doi:10.1029/2008GL033666.

Lin, N., H. U. Frey, S. B. Mende, F. S. Mozer, R. L. Lysak, Y. Song, and V. Angelopoulos (2009), Statistical study of substorm timing sequence, *J. Geophys. Res.*, *114*, A12204, doi:10.1029/2009JA014381.

Lui, A. T. Y. (1996), Current disruption in the Earth's magnetosphere: Observations and models, *J. Geophys. Res.*, *101*, 13,067–13,088, doi:10.1029/96JA00079.

Lui, A. T. Y., R. E. Lopez, B. J. Anderson, K. Takahashi, L. J. Zanetti, R. W. McEntire, T. A. Potemra, D. M. Klumpar, E. M. Greene, and R. Strangeway (1992), Current disruptions in the near-Earth neutral sheet region, *J. Geophys. Res.*, *97*(A2), 1461–1480, doi:10.1029/91JA02401.

Lyons, L. R., I. O. Voronkov, E. F. Donovan, and E. Zesta (2002), Relation of substorm breakup arc to other growth-phase auroral arcs, *J. Geophys. Res.*, *107*(A11), 1390, doi:10.1029/2002JA009317.

McPherron, R. L., C. T. Russell, and M. P. Aubry (1973), Satellite studies of magnetospheric substorms on August 15, 1968: 9. Phenomenological model for substorms, *J. Geophys. Res.*, *78*(16), 3131–3149, doi:10.1029/JA078i016p03131.

Mende, S. B., C. W. Carlson, H. U. Frey, T. J. Immel, and J.-C. Gérard (2003), IMAGE FUV and in situ FAST particle observations of substorm aurorae, *J. Geophys. Res.*, *108*(A4), 8010, doi:10.1029/2002JA009413.

Miyashita, Y., et al. (2009), A state-of-the-art picture of substorm-associated evolution of the near-Earth magnetotail obtained from superposed epoch analysis, *J. Geophys. Res.*, *114*, A01211, doi:10.1029/2008JA013225.

Nagai, T. (1982), Observed magnetic substorm signatures at synchronous altitude, *J. Geophys. Res.*, *87*(A6), 4405–4417, doi:10.1029/JA087iA06p04405.

Nagai, T., M. Fujimoto, Y. Saito, S. Machida, T. Terasawa, R. Nakamura, T. Yamamoto, T. Mukai, A. Nishida, and S. Kokubun (1998), Structure and dynamics of magnetic reconnection for substorm onsets with Geotail observations, *J. Geophys. Res.*, *103*(A3), 4419–4440, doi:10.1029/97JA02190.

Nakamura, R., A. Retinò, W. Baumjohann, M. Volwerk, N. Erkaev, B. Klecker, E. A. Lucek, I. Dandouras, M. André, and Y. Khotyaintsev (2009), Evolution of dipolarization in the near-Earth current sheet induced by Earthward rapid flux transport, *Ann. Geophys.*, *27*, 1743–1754, doi:10.5194/angeo-27-1743-2009.

Nishida, A., and E. W. Hones Jr. (1974), Association of plasma sheet thinning with neutral line formation in the magnetotail, *J. Geophys. Res.*, *79*(4), 535–547, doi:10.1029/JA079i004p00535.

Ohtani, S., S. Kokubun, and C. T. Russell (1992), Radial expansion of the tail current disruption during substorms: A new approach to the substorm onset region, *J. Geophys. Res.*, *97*(A3), 3129–3136, doi:10.1029/91JA02470.

Ohtani, S., M. A. Shay, and T. Mukai (2004), Temporal structure of the fast convective flow in the plasma sheet: Comparison between observations and two-fluid simulations, *J. Geophys. Res.*, *109*, A03210, doi:10.1029/2003JA010002.

Petrukovich, A. A., W. Baumjohann, R. Nakamura, A. Runov, A. Balogh, and H. Rème (2007), Thinning and stretching of the plasma sheet, *J. Geophys. Res.*, *112*, A10213, doi:10.1029/2007JA012349.

Petrukovich, A. A., W. Baumjohann, R. Nakamura, and H. Rème (2009), Tailward and earthward flow onsets observed by Cluster in a thin current sheet, *J. Geophys. Res.*, *114*, A09203, doi:10.1029/2009JA014064.

Rae, I. J., et al. (2009), Near-Earth initiation of a terrestrial substorm, *J. Geophys. Res.*, *114*, A07220, doi:10.1029/2008JA013771.

Runov, A., V. Angelopoulos, M. I. Sitnov, V. A. Sergeev, J. Bonnell, J. P. McFadden, D. Larson, K.-H. Glassmeier, and U. Auster (2009), THEMIS observations of an earthward-propagating dipolarization front, *Geophys. Res. Lett.*, *36*, L14106, doi:10.1029/2009GL038980.

Samson, J. C., L. R. Lyons, P. T. Newell, F. Creutzberg, and B. Xu (1992), Proton aurora and substorm intensifications, *Geophys. Res. Lett.*, *19*(21), 2167–2170, doi:10.1029/92GL02184.

Sanny, J., R. L. McPherron, C. T. Russell, D. N. Baker, T. I. Pulkkinen, and A. Nishida (1994), Growth-phase thinning of the near-Earth current sheet during the CDAW 6 substorm, *J. Geophys. Res.*, *99*(A4), 5805–5816, doi:10.1029/93JA03235.

Semenov, V. S., T. Penz, V. V. Ivanova, V. A. Sergeev, H. K. Biernat, R. Nakamura, M. F. Heyn, I. V. Kubyshkin, and I. B. Ivanov (2005), Reconstruction of the reconnection rate from Cluster measurements: First results, *J. Geophys. Res.*, *110*, A11217, doi:10.1029/2005JA011181.

Sergeev, V., R. C. Elphic, F. S. Mozer, A. Saint-Marc, and J.-A. Sauvaud (1992), A two-satellite study of nightside flux transfer events in the plasma sheet, *Planet. Space Sci.*, *40*, 1551–1572, doi:10.1016/0032-0633(92)90052-P.

Sergeev, V. A., D. G. Mitchell, C. T. Russell, and D. J. Williams (1993), Structure of the tail plasma/current sheet at ~11 R_E and its changes in the course of a substorm, *J. Geophys. Res.*, *98*(A10), 17,345–17,365, doi:10.1029/93JA01151.

Sergeev, V. A., N. P. Dmitrieva, E. E. Timofeev, K. Liou, Y. Miyashita, T. Mukai, and T. Pulkkinen (2004), Strong control of auroral precipitation by the plasma sheet parameters and the problem of pseudobreakups, in *Seventh International Conference on Substorm*, *Rep. 2004:5*, edited by N. Ganushkina and T. Pulkkinen, pp. 182–185, Finn. Meteorol. Inst., Helsinki, 2004.

Sergeev, V. A., et al. (2005), Transition from substorm growth to substorm expansion phase as observed with a radial configuration of ISTP and Cluster spacecraft, *Ann. Geophys.*, *23*, 2183–2198, doi:10.5194/angeo-23-2183-2005.

Sergeev, V., et al. (2008), Study of near-Earth reconnection events with Cluster and Double Star, *J. Geophys. Res.*, *113*, A07S36, doi:10.1029/2007JA012902.

Sharma, A. S., et al. (2008), Transient and localized processes in the magnetotail: A review, *Ann. Geophys.*, *26*, 955–1006, doi:10.5194/angeo-26-955-2008.

Shiokawa, K., et al. (1998), High-speed ion flow, substorm current wedge, and multiple Pi 2 pulsations, *J. Geophys. Res.*, *103*(A3), 4491-4507, doi:10.1029/97JA01680.

Slavin, J. A., E. I. Tanskanen, M. Hesse, C. J. Owen, M. W. Dunlop, S. Imber, E. A. Lucek, A. Balogh, and K.-H. Glassmeier (2005), Cluster observations of traveling compression regions in the near-tail, *J. Geophys. Res.*, *110*, A06207, doi:10.1029/2004JA010878.

Tsyganenko, N. A., and T. Mukai (2003), Tail plasma sheet models derived from Geotail particle data, *J. Geophys. Res.*, *108*(A3), 1136, doi:10.1029/2002JA009707.

Wolf, R. A., Y. Wan, X. Xing, J.-C. Zhang, and S. Sazykin (2009), Entropy and plasma sheet transport, *J. Geophys. Res.*, *114*, A00D05, doi:10.1029/2009JA014044.

Xing, X., L. R. Lyons, V. Angelopoulos, D. Larson, C. Carlson, A. Runov, and U. Auster (2010), Plasma sheet pressure evolution related to substorms, *J. Geophys. Res.*, *115*, A01212, doi:10.1029/2009JA014315.

Yahnin, A. G., et al. (2001), Correlated Interball/ground-based observations of isolated substorm: The pseudo-breakup phase, *Ann. Geophys.*, *19*, 687–698, doi:10.5194/angeo-19-687-2001.

Zhou, X.-Z., V. Angelopoulos, V. A. Sergeev, and A. Runov (2010), Accelerated ions ahead of earthward propagating dipolarization fronts, *J. Geophys. Res.*, *115*, A00I03, doi:10.1029/2010JA015481.

V. Angelopoulos, A. Runov, and X.-Z. Zhou, Institute of Geophysics and Planetary Physics, University of California, Box 951567, Los Angeles, CA 90095, USA.

E. Donovan, Department of Physics and Astronomy, University of Calgary, Calgary, AB T2N 1N4, Canada.

M. Kubyshkina and V. Sergeev, Institute of Physics, St. Petersburg State University, St. Petersburg 198504, Russia. (victor@geo.phys.spbu.ru)

J. McFadden, Space Science Laboratory, University of California, 7 Gauss Way, Berkeley, CA 94720, USA.

R. Nakamura, Space Research Institute, Austrian Academy of Sciences, Schmiedlstrasse 6, A-8042 Graz, Austria.

H. Singer, NOAA Space Weather Prediction Center, 325 Broadway, Boulder, CO 80303, USA.